Mechanics of Advanced Composite Structures 9 (2022) 399 – 408
This is an Open Access paper licensed under the Creative Commons License CC-BY 4.0 license

Semnan University

Mechanics of Advanced Composite Structures

journal homepage: http://MACS.journals.semnan.ac.ir

A Case Study on the Influence of Friction Coefficient and Rotational Speed on Transient Thermoelastic Response of FGM Rotating Cylinder

R. Koohi Faegh [a], M. Omidi Bidgoli[b,c*], Mohammad Hosseini[d]

[a] *Department of Machinery Nasb Niroo Co (Mapna group), Iran*
[b] *Department of Mechanical Engineering, University of Eyvanekey, Eyvanekey 99888-35918, Iran*
[c] *Department of Mechanical Engineering, Islamic Azad University, Badroud Branch, Badroud, Iran*
[d] *Department of Mechanical Engineering, University of Hormozgan, Bandar Abbas, Iran.*

KEYWORDS

Friction;
Rotational speed;
Thermoelastic response;
Functionally graded material;
Rotating cylinder.

ABSTRACT

The effect of friction and rotational speed parameters changes on the transient thermoelastic response of a rotating functionally graded cylinder with a short length subjected to thermal and mechanical loads are studied based on the First order shear deformation theory (FSDT). It is assumed that the cylinder is located on a friction bed and is rotating due to an external torque. The material property is assumed to be variable along radius according to a volume fraction distribution. Because temperature changes are unstable the changes in parameters are applied when the cylinder has reached a steady state. In the following, radial, longitudinal and angular displacement diagrams, as well as effective stresses due to changes in coefficient of friction and rotational velocities for longitudinal and radial directions, are drawn. The results show that these changes have significant effects on the measured parameters and in many industrial applications, these coefficients are not constant during the work period and have changed.

1. Introduction

Rotating shells are classified by their geometry (cylindrical, spherical, etc.) a shell is a thin structure composed of curved sheets of material so that the curvature plays an important role in the structural behavior. Today, these structures have many applications in the oil, gas, and petrochemical industries, military and aerospace industries, turbines, and reactors. On the other hand, with the rapid advancement of technology, the need to use new materials as engineering priorities in high-efficiency complex systems has been raised. Functionally graded materials are non-homogeneous composites composed of two or more different materials, and the composition of the constituent components varies continuously and in the form of a function of position in one or more specific regions [1, 2]. Gradual and continuous changes in physical properties can be useful to work in different environments and at very high temperatures. Functionally graded materials are used in modern technologies [3-5] for structural components such as those used in, nuclear, aircraft, space engineering, and pressure vessels. Different types of FGM, such as materials under the power distribution law or volume fraction and exponential distribution law, have led researchers to analyze structures with different target structures [6-8]. In many of these structures, the need to simultaneously provide material resistance to different thermal and mechanical loads and considering the physical properties of these materials in thermoelastic equilibrium causes the complexity of the structural equation analysis, which necessitates the choice of the appropriate method for thermoelastic analysis [9, 10].

An exact analysis of an axial compressor's spool of a gas turbine engine for both homogeneous and functionally graded material states and spool subjected to centrifugal force and uniform radial loadings at internal and external surfaces to calculate stresses, strains, and displacements was presented by Yousefi *et al.* [11]. In the other research, Shahriari *et al.* [12] suggested a model in the framework of rotating a

* Corresponding author. Tel.: +98-9132604478
E-mail address: mostafaomidibidgoli@gmail.com

DOI: 10.22075/macs.2022.24906.1362
Received 2021-10-16; Received in revised form 2022-08-13; Accepted 2022-09-20.
© 2022 Published by Semnan University Press. All rights reserved.

thick-walled hollow circular cylinder with free-clamp ends under centrifugal load for analysis of compressors spool in a turbojet engine. Lezgy-Nazargah and Meshkani [13] present a finite element solution for static and free vibration analysis of functionally graded material plates rested on Winkler-Pasternak elastic foundations. A new analysis of functionally graded piezoelectric laminates based on simplifying the assumption that the FGP layer consists of several homogeneous sub-layers was introduced by Lezgy-Nazargah [14]. A three-dimensional exact state-space solution for cylindrical bending of continuously non-homogenous piezoelectric laminated plates with arbitrary gradient composition was presented by Lezgy-Nazargah [15]. Based on the finite element method, Lezgy-Nazargah [16] studied the fully coupled thermo-mechanical behavior of bi-directional FGM beam structures. Arefi [17] presented thermoelastic analyses of functionally graded cylindrical shells by using generalized shear deformation theory. Akbarzadeh and Chen [18] obtained analytical solutions for multi-physical responses of an FG, thermomagneto-elastic rotating hollow cylinder as well as a homogeneous orthotropic thermo-magneto-electro-elastic Cylinder. Nonlinear analysis of varying thickness cylindrical shells with moderately large deformation subjected to non-uniform pressure using first-order shear deformation theory was presented by Nasrekani *et al*. [19]. Ghannad and Parhizkar Yaghoobi [20] presented a Thermo-elasticity solution for thick cylinders under thermo-mechanical loads with various boundary conditions.

Thermo-elastic behavior of axially functionally graded rotating thick cylindrical shells with variable thickness under mechanical loading was investigated by Jabbari *et al*. [21]. Thermoelastic analysis of clamped-clamped thick FGM cylinders using third-order shear deformation theory was considered by Gharooni *et al*. [22]. 2D thermo-elastic behavior of an FG cylinder under thermomechanical loads was considered by Ghannad *et al*. [23] using a first-order temperature theory. Nonsymmetrical thermo-mechanical analysis of a functionally graded cylinder subjected to mechanical, thermal, and magnetic loads was presented by Loghman *et al*. [24]. Omidi *et al*. [25] analysis of thermo-elastic behavior of FGM rotating cylinder resting on friction bed subjected to a thermal gradient and an external torque. Effect of grading index on two-dimensional stress and strain distribution of FG rotating cylinder resting on a friction bed under thermo-mechanical loads studied by Omidi *et al*. [26]. Omidi *et al*. [27], presented a three-dimensional thermo-elastic analysis of a rotating cylindrical functionally graded shell subjected to the mechanical and thermal loads based on the FSDT formulation. Omidi *et al*. [28] researched transient stresses and deformation analysis of a shear deformable functionally graded rotating cylindrical shell made of Al-SiC subjected to thermo-mechanical loading.

The influence of friction coefficient and rotational speed on the transient thermo-elastic response of cylindrical FGM isn't investigated in previous research. In this paper, the effect of changes in coefficient of friction and rotational slip on the thermo-elastic behavior of Al-SiC cylindrical shell has been investigated and analyzed. Radial and axial distributions of the effective stress for different friction coefficients and different rotating speeds were determined. On the other hand, the use of volume fraction is one of the innovations of this article. Many articles have been presented about power distribution or exponential functions, but fewer articles have been presented about volume fractions. Another reason for using volume fraction is its greater compatibility with the properties of composites.

2. Problem Formulation

An FG rotating cylinder with an inner radius R_i, outer radius R_o, and axial length L that is subjected to internal and external pressure and temperature (P_i, P_o, T_i, T_o) is shown in Fig.1. The cylinder is made from a mixture of ceramic and metal and is defined in the cylindrical coordinate system (r, x, θ).

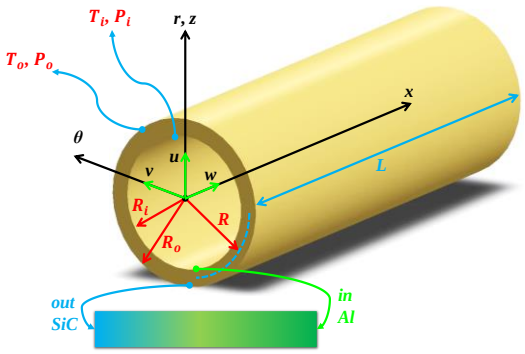

Fig. 1. The schematic of a cylindrical shell and Particle distribution along the radius.

The properties of a functionally graded material are considered by using the volume fraction distribution as follows [29]:

$$P = (P_c - P_m)\left(\frac{2r+h}{2h}\right)^n + P_m \tag{1}$$

where

$$P_c = \text{material property of ceramic}$$
$$P_m = \text{material property of metal} \tag{2}$$

The FG material is distributed around the mid-radius of the cylinder. Material properties are assumed based on volume fraction distribution as follows:

$$\begin{aligned} E &= (E_c - E_m)(\frac{2r+h}{2h})^n + E_m \\ \alpha &= (\alpha_c - \alpha_m)(\frac{2r+h}{2h})^n + \alpha_m \\ k &= (k_c - k_m)(\frac{2r+h}{2h})^n + k_m \\ \rho &= (\rho_c - \rho_m)(\frac{2r+h}{2h})^n + \rho_m \\ c &= (c_c - c_m)(\frac{2r+h}{2h})^n + c_m \end{aligned} \quad (3)$$

2.1. Thermal Solution

The temperature distribution is obtained using the solution of the heat conduction equation as follows:

$$\frac{1}{r}\frac{\partial}{\partial r}\left(kr\frac{\partial T}{\partial r}\right) + \dot{q} = \rho c \frac{\partial T}{\partial t} \quad (4)$$

Considering the heat due to friction, the initial and thermal boundary conditions are:

$$I.C. = T(r,0) = 27^0 c \quad (5)$$

$$B.C. \begin{cases} r = r_i \Rightarrow T_s(r_i,t) = T_i \\ r = r_o \Rightarrow -k\left.\frac{\partial T_s}{\partial r}\right|_{r_o} = h(T_s - T_o) \end{cases} \quad (6)$$

In the general solution by assuming $\dot{q} = 0$, $T(r,t)$ is obtained as follows:

$$T(r,t) = T_s(r) + T_h(r,t) \quad (7)$$

that $T_s(r)$ and $T_h(r,t)$ are the steady-state solution and the transient solution respectively. Before obtaining $T(r,t)$, we need to calculate the heat transfer coefficient (h).

To calculate the heat transfer coefficient with the assumption of mineral oil, we have:

$$\bar{h} = 0.037 \times \mathrm{Re}^{0.8} \times \mathrm{Pr}^{1/3} \times \frac{k}{L} \quad (8)$$

If the thickness of the oil film is assumed to be 1*mm* and the diameter of the cylinder is 360 *mm* (due to the very small ratio of thickness to diameter), the assumption of a flat plate is correct and acceptable. Here the rotational speed of the cylinder is 3200 *rpm*.

$$\omega = 3200 \times \frac{2\pi}{60} = 334 rps \quad (9)$$

The schematic of the plate is shown in Fig. 2.

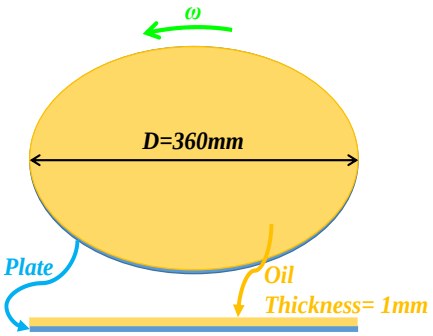

Fig. 2. Flat Plate Condition.

Therefore, the linear velocity of the cylinder edge is:

$$V = r \times \omega = 0.18 \times 334 = 60.12 \, m/s \quad (10)$$

By selecting mineral oil with a density of $870 \, kg/m^3$, the Reynolds number is:

$$\mathrm{Re} = \frac{\rho V L}{\mu} = \frac{870 \times 60.12 \times 2\pi \times 0.18}{17 \times 10^{-3}} = 3479699 \quad (11)$$

Because the resulted Reynolds value is greater than 5×10^5 the flow is turbulent. On the other hand, the value of the Nusselt number on the flat plate for turbulent flow is equal to:

$$\begin{aligned} \overline{NU} &= \frac{\bar{h} \times L}{k} = 0.037 \times \mathrm{Re}^{0.8} \times \mathrm{Pr}^{1/3} \\ \Rightarrow \bar{h} &= 0.037 \times \mathrm{Re}^{0.8} \times \mathrm{Pr}^{1/3} \times \frac{k}{L} \end{aligned} \quad (12)$$

We also have for the mentioned oil:

$$\mathrm{Pr} = \frac{C_p \times \mu}{k} = \frac{2100 \times 17 \times 10^{-3}}{0.14} = 255 \quad (13)$$

As a result:

$$\begin{aligned} \bar{h} &= 0.037 \times \mathrm{Re}^{0.8} \times \mathrm{Pr}^{1/3} \times \frac{k}{L} \\ \Rightarrow \bar{h} &= 0.037 \times (3479699)^{0.8} \times (255)^{1/3} \times \frac{0.14}{2\pi \times 0.1} \\ \rightarrow h &= 4969 \frac{W}{m^2 K} \end{aligned} \quad (14)$$

Now if we consider the right side of Eq. (4) equal to zero, the solution of the equation of uniform temperature distribution of the cylinder is as follows:

$$\begin{aligned} &\frac{1}{r}\left(\frac{\partial}{\partial r}\left(kr\frac{\partial T_s}{\partial r}\right)\right) = 0 \\ &\Rightarrow T_s(r) = c_1 \int \frac{1}{kr} dr + c_2 \end{aligned} \quad (15)$$

Using Eq. (3), the volume fraction distribution coefficient of thermal conductivity is considered as follows:

$$\begin{aligned} & k=(k_c-k_m)(\frac{r-r_i}{r_o-r_i})^2+k_m \\ & \rightarrow k=\frac{k_c-k_m}{(r_o-r_i)^2}r^2-2r_i\frac{k_c-k_m}{(r_o-r_i)^2}r \\ & \quad +(k_m+\frac{k_c-k_m}{(r_o-r_i)^2}(r_i^2) \end{aligned} \tag{16}$$

that T_s is obtained as follows:

$$T_s(r)=c_1\begin{pmatrix}\frac{1}{\Theta_3}\ln(r)+\\ \frac{1}{\Theta_3}\begin{pmatrix}\left(\frac{\Theta_2-\Theta_1\Delta_1}{\Delta_1-\Delta_2}\right)\ln(r-\Delta_1)\\ +\begin{pmatrix}-\Theta_1\\ -\left(\frac{\Theta_2-\Theta_1\Delta_1}{\Delta_1-\Delta_2}\right)\end{pmatrix}\ln(r-\Delta_2)\end{pmatrix}\end{pmatrix}+c_2 \tag{17}$$

The parameters appeared in Eq. (5) are defined as:

$$\begin{cases}\Theta_1=\dfrac{k_c-k_m}{(r_o-r_i)^2}\\ \Theta_2=(2r_i)\dfrac{k_c-k_m}{(r_o-r_i)^2}\\ \Theta_3=k_m+\dfrac{k_c-k_m}{(r_o-r_i)^2}(r_i)^2\\ \Delta_1=\dfrac{b+\sqrt{b^2-4ac}}{2a}\\ \Delta_2=\dfrac{b-\sqrt{b^2-4ac}}{2a}\end{cases} \tag{18}$$

By using the boundary condition, the integration constants c_1 and c_2 are obtained as:

$$\begin{cases}c_1=\dfrac{h(T_i-T_o)}{-k_{r_o}B(r_o)+h(A(r_i)-A(r_o))}\\ c_2=T_i-\dfrac{h(T_i-T_o)}{-k_{r_i}B(r_o)+h(A(r_i)-A(r_o))}A(r_i)\end{cases} \tag{19}$$

in which:

$$\begin{aligned} & A(r)=\frac{1}{\Theta_3}\ln(r)+\frac{1}{\Theta_3}\begin{pmatrix}\left(\frac{\Theta_2-\Theta_1\Delta_1}{\Delta_1-\Delta_2}\right)\ln(r-\Delta_1)\\ +\begin{pmatrix}-\Theta_1\\ -\left(\frac{\Theta_2-\Theta_1\Delta_1}{\Delta_1-\Delta_2}\right)\end{pmatrix}\ln(r-\Delta_2)\end{pmatrix} \\ & B(r)=\Theta_1r^3-\Theta_2r^2+\Theta_3r \end{aligned} \tag{20}$$

Next, if the right-hand side of Equation (4) doesn't time zero, the solution of the non-uniform temperature distribution is given $(T(r,t))$. Here we have an Advection-Diffusion Equation:

$$\begin{aligned} & \frac{1}{r}\frac{\partial}{\partial r}\left(kr\frac{\partial T}{\partial r}\right)=\rho c\frac{\partial T}{\partial t} \\ & \rightarrow \frac{k}{r}T_r+kT_{rr}=\rho cT_t \\ & \rightarrow T_t+\left(-\frac{k}{r\rho c}\right)T_r=\left(\frac{k}{\rho c}\right)T_{rr} \\ & \Rightarrow T_t+uT_r=\alpha T_{rr} \end{aligned} \tag{21}$$

At first:

$$\begin{cases}r=R+Z\\ r_i=R-\dfrac{h}{2}\\ r_o=R+\dfrac{h}{2}\end{cases} \tag{22}$$

$$\Rightarrow\begin{cases}k=(k_c-k_m)(\dfrac{r-r_i}{r_o-r_i})^2+k_m\\ \rho=(\rho_c-\rho_m)(\dfrac{r-r_i}{r_o-r_i})^2+\rho_m\\ c=(c_c-c_m)(\dfrac{r-r_i}{r_o-r_i})^2+c_m\end{cases}$$

By replacing the above values in the heat transfer equation in the cylindrical coordinate system, we have:

$$\begin{aligned} & \frac{1}{r}\left[kr\frac{\partial^2T}{\partial r^2}+\left[k_m+\frac{k_c-k_m}{(r_o-r_i)^2}(2r-r_i)^2\right]\frac{\partial T}{\partial r}\right] \\ & =\rho c\frac{\partial T}{\partial t} \end{aligned} \tag{23}$$

Also, the product of density in specific heat capacity is equal to:

$$\begin{aligned} \rho c=&(\rho_c-\rho_m)(c_c-c_m)(\frac{r-r_i}{r_o-r_i})^4 \\ &+(\rho_c-\rho_m)c_m(\frac{r-r_i}{r_o-r_i})^2 \\ &+(c_c-c_m)\rho_m(\frac{r-r_i}{r_o-r_i})^2+\rho_mc_m \end{aligned} \tag{24}$$

The equation of final non-uniform temperature distribution for a cylinder with volume fraction distribution is written as follows:

$$\frac{\partial^2T}{\partial r^2}+\left(\frac{1}{r}+\frac{k'(r)}{k(r)}\right)\frac{\partial T}{\partial r}=\frac{\rho c}{k}\frac{\partial T}{\partial t} \tag{25}$$

Now to solve the above equation, we used the finite difference method:

$$\begin{cases}\dfrac{\partial^2T}{\partial r^2}=\dfrac{T_{j+1}+T_{j-1}-2T_j}{(\Delta r)^2}\\ \dfrac{\partial T}{\partial r}=\dfrac{T_{j+1}-T_j}{\Delta r}\\ \dfrac{\partial T}{\partial t}=\dfrac{T_j^{(t)}-T_j^{(t-1)}}{\Delta t}\end{cases} \tag{26}$$

For this purpose, the solution domain is divided into some finite divisions (as shown in Fig. 3).

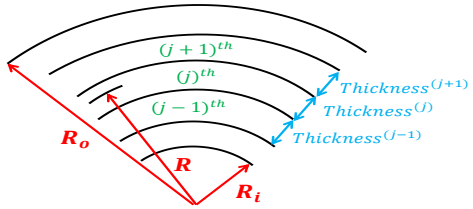

Fig. 3. Dividing radial domain into some finite sub-domains.

By replacing the above values in Eq. (24) we have:

$$\frac{T_{j+1}^{(t)}+T_{j-1}^{(t)}-2T_j^{(t)}}{(\Delta r)^2}+\left[\frac{1}{r_j}+\frac{k'(r_j)}{k(r_j)}\right]\frac{T_{j+1}^{(t)}-T_j^{(t)}}{\Delta r}=\frac{\rho(r_j)c(r_j)}{k(r_j)}\frac{T_j^{(t)}-T_j^{(t-1)}}{\Delta t} \tag{27}$$

Based on the finite difference method, Eq. (27) is rewritten as:

$$\begin{aligned}&\frac{1}{(\Delta r)^2}T_{j+1}^{(t)}+\frac{1}{(\Delta r)^2}T_{j-1}^{(t)}-\frac{2}{(\Delta r)^2}T_j^{(t)}\\&+\frac{1}{\Delta r}\left(\frac{1}{r_j}+\frac{k'(r_j)}{k(r_j)}\right)T_{j+1}^{(t)}\\&-\frac{1}{\Delta r}\left(\frac{1}{r_j}+\frac{k'(r_j)}{k(r_j)}\right)T_j^{(t)}\\&-\frac{\rho(r_j)c(r_j)}{k(r_j)}\frac{1}{\Delta t}T_j^{(t)}\\&=-\frac{1}{\Delta t}\frac{\rho(r_j)c(r_j)}{k(r_j)}T_j^{(t-1)}\end{aligned} \tag{28}$$

$$\begin{aligned}&-\frac{(\Delta t)k(r_j)}{\rho(r_j)c(r_j)}\left[\frac{1}{(\Delta r)^2}+\frac{1}{\Delta r}\left[\frac{1}{r_j}+\frac{k'(r_j)}{k(r_j)}\right]\right]T_{j+1}^{(t)}\\&+\frac{(\Delta t)k(r_j)}{\rho(r_j)c(r_j)}\left[\frac{2}{(\Delta r)^2}+\frac{1}{\Delta r}\left[\frac{1}{r_j}+\frac{k'(r_j)}{k(r_j)}\right]+\frac{\rho(r_j)c(r_j)}{(\Delta t)k(r_j)}\right]T_j^{(t)}\\&-\frac{(\Delta t)k(r_j)}{\rho(r_j)c(r_j)}\left[\frac{1}{(\Delta r)^2}\right]T_{j-1}^{(t)}=T_j^{(t-1)}\end{aligned} \tag{29}$$

In Eq. (29) it is assumed;

$$\begin{aligned}a_j&=-\frac{(\Delta t)k(r_j)}{\rho(r_j)c(r_j)}\left[\frac{1}{(\Delta r)^2}\right]\\b_j&=\frac{(\Delta t)k(r_j)}{\rho(r_j)c(r_j)}\left[\frac{2}{(\Delta r)^2}+\frac{1}{\Delta r}\left[\frac{1}{r_i}+\frac{k'(r_j)}{k(r_j)}\right]+\frac{\rho(r_j)c(r_j)}{(\Delta t)k(r_j)}\right]\\d_j&=-\frac{(\Delta t)k(r_j)}{\rho(r_j)c(r_j)}\left[\frac{1}{(\Delta r)^2}+\frac{1}{\Delta r}\left[\frac{1}{r_j}+\frac{k'(r_j)}{k(r_j)}\right]\right]\end{aligned} \tag{30}$$

Finally, we can consider the following relation:

$$a_jT_{j-1}^{(t)}+b_jT_j^{(t)}+d_jT_{j+1}^{(t)}=T_j^{(t-1)}\left(j=1,2,\cdots,N-1,N\right) \tag{31}$$

and the boundary condition writes as follows:

$$B.C.\begin{cases}T_1=T_i\\-k_{r_o}\dfrac{T_N-T_{N-1}}{(\Delta r)}=hT_N-hT_o\\\Rightarrow T_N=\dfrac{\frac{k_{r_o}}{\Delta r}}{\frac{k_{r_o}}{\Delta r}+h}T_{N-1}+\dfrac{h}{\frac{k_{r_o}}{\Delta r}+h}T_o\end{cases} \tag{32}$$

Now by applying the thermal boundary conditions we have:

$$\begin{aligned}&j=2:b_2T_2^{(t)}+d_2T_3^{(t)}=T_2^{(t-1)}-a_2T_i\\&j=3:a_3T_2^{(t)}+b_3T_3^{(t)}+d_3T_4^{(t)}=T_3^{(t-1)}\\&j=4:a_4T_3^{(t)}+b_4T_4^{(t)}+d_4T_5^{(t)}=T_4^{(t-1)}\\&j=N-1:a_{N-1}T_{N-2}^{(t)}+b_{N-1}T_{N-1}^{(t)}+d_{N-1}T_N^{(t)}=T_{N-1}^{(t-1)}\\&\rightarrow a_{N-1}T_{N-2}^{(t)}+\left[b_{N-1}+\frac{\frac{k_{r_o}}{\Delta r}}{\frac{k_{r_o}}{\Delta r}+h}d_{N-1}\right]T_{N-1}^{(t)}\\&=T_{N-1}^{(t-1)}-\left[\frac{hT_o}{\frac{k_{r_o}}{\Delta r}+h}\right]d_{N-1}\end{aligned} \tag{33}$$

$$\begin{bmatrix}b_2&d_2&0&0&0\\a_3&a_3&d_3&0&0\\0&a_4&b_4&d_4&0\\0&0&a_5&b_5&d_5\\&&&\ddots&\\&&&a_{N-1}&b_{N-1}+\dfrac{\frac{k_{r_o}}{\Delta r}}{\frac{k_{r_o}}{\Delta r}+h}d_{N-1}\end{bmatrix}_{(N-2)\times(N-2)}\begin{bmatrix}T_2\\T_3\\T_4\\T_5\\\vdots\\T_{N-2}\\T_{N-1}\end{bmatrix}=\begin{bmatrix}T_2^{(t-1)}-a_2T_i\\T_3^{(t-1)}\\T_4^{(t-1)}\\T_5^{(t-1)}\\\vdots\\T_{N-2}\\T_{N+1}^{(t-1)}-\left[\dfrac{hT_o}{\frac{k_{r_o}}{\Delta r}+h}\right]d_{N+1}\end{bmatrix} \tag{34}$$

Next, if we write the above equations as a matrix, we have Equation (34).

After solving, the unknown matrix is calculated as follows:

$$AX = B \rightarrow X = A^{-1}B \rightarrow X = \frac{B}{A} \tag{35}$$

The finite difference method also is used to solve the heat conduction problem. Figure 4 shows the radial and axial distribution of transient temperature at various times. It is observed that with the increase of time, the radial distribution of temperature is tending to be uniform. The initial and boundary conditions are completely satisfied based on these results.

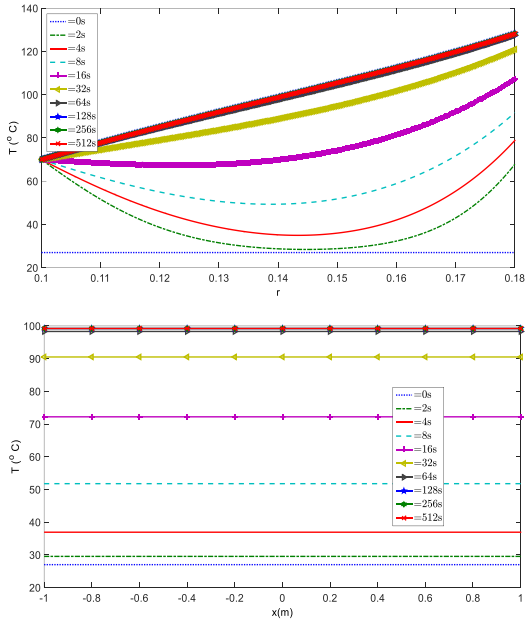

Fig. 4. The radial and axial distribution of temperature for various times.

2.2. Thermoelastic Solution

Thermo-elastic relations are developed in this section. Based on the FSDT, displacement components are considered as a linear combination of displacement of mid-surface and rotation about mid-surface. For a symmetric analysis, the displacement field is written as:

$$\begin{Bmatrix} U_z(x,\theta) \\ W_x(x,\theta) \\ V_\theta(x,\theta) \end{Bmatrix} = \begin{Bmatrix} u(x,\theta) \\ w(x,\theta) \\ v(x,\theta) \end{Bmatrix} + z \begin{Bmatrix} \phi_z(x,\theta) \\ \phi_x(x,\theta) \\ \phi_\theta(x,\theta) \end{Bmatrix} \tag{36}$$

Using the strain-displacement relations, and the generalized Hooke's law, strain energy per unit volume of the FG cylindrical shell is obtained as:

$$\begin{aligned} \bar{u} &= \frac{1}{2}\{\varepsilon\}^T\{\sigma\} = \frac{1}{2}\begin{Bmatrix} \sigma_{zz}\varepsilon_{zz} + \sigma_{\theta\theta}\varepsilon_{\theta\theta} + \sigma_{xx}\varepsilon_{xx} \\ +\tau_{zx}\varepsilon_{zx} + \tau_{z\theta}\varepsilon_{z\theta} + \tau_{x\theta}\varepsilon_{x\theta} \end{Bmatrix} \\ \rightarrow \bar{u} &= \frac{1}{2}\frac{E}{(1+\nu)(1-2\nu)}\Big[(1-\nu)\left(\varepsilon_{zz}^2 + \varepsilon_{\theta\theta}^2 + \varepsilon_{xx}^2\right) \\ &\quad + 2\nu\left(\varepsilon_{zz}\varepsilon_{\theta\theta} + \varepsilon_{zz}\varepsilon_{xx} + \varepsilon_{\theta\theta}\varepsilon_{xx}\right) \\ &\quad - (1+\nu)\alpha(z)T\left(\varepsilon_{zz} + \varepsilon_{\theta\theta} + \varepsilon_{xx}\right) \\ &\quad + \frac{k(1-2\nu)}{2}\left(\gamma_{zx}^2 + \gamma_{z\theta}^2 + \gamma_{x\theta}^2\right)\Big] \end{aligned} \tag{37}$$

In a more simple form, the total energy is presented as a combination of mechanical and thermal energies as follows:

$$\begin{aligned} U &= \int_0^L \left[U_s(x) - U_T(x)\right]dx \\ U_s(x) &= \sum_{i=1}^{9} A_i(x) f_i(x) \\ \rightarrow f_i(x) &= f_i(u, w, v, \phi_z, \phi_x, \phi_\theta) \\ U_T(x) &= \sum_{i=1}^{9} B_i(x) g_i(x) \\ \rightarrow g_i(x) &= g_i(u, w, \phi_z, \phi_x) \end{aligned} \tag{38}$$

in which $A_i(x), f_i(x), B_i(x), g_i(x)$, are functions of $(u, w, v, \phi_z, \phi_x, \phi_\theta)$ and material properties. In continuation, the external works are calculated as:

$$\begin{aligned} W_1 &= 2\pi\int_0^L \left[P_i r_i - P_o r_o\right]u + \frac{h}{2}\left(-P_i r_i - P_o r_o\right)\phi_z d_X \\ \Rightarrow W_1 &= \int_0^L (d_1 u + d_2\phi_z)dx \\ d_1 &= 2\pi\left(P_i(x) r_i - P_o(x) r_o\right) \\ d_2 &= 2\pi\left(\frac{h}{2}\right)\left(-P_i(x) r_i - P_o(x) r_o\right) \end{aligned} \tag{39}$$

The work due to rotation of cylindrical shell is obtained as:

$$\begin{aligned} W_2 &= 2\pi\int_0^L \int_{-\frac{h}{2}}^{+\frac{h}{2}} \begin{bmatrix} \left(\rho(z)(R+z)^2\omega^2\right)u \\ +\left(\rho(z)(R+z)^2\omega^2 z\right)\phi_z \end{bmatrix} dz dx \\ \rightarrow W_2 &= \int_0^L \left(H_1 u + H_2\phi_z\right)dx \\ H_1 &= 2\pi\omega^2\begin{bmatrix} (\rho_c - \rho_m)\left(\frac{h^3}{30} + \frac{Rh^2}{6} + \frac{R^2 h}{3}\right) \\ +\rho_m\left(\frac{h^3}{12} + R^2 h\right) \end{bmatrix} \end{aligned} \tag{40}$$

and the external work due to friction is obtained as:

$$W_3 = -\int_0^{2\pi}\int_0^L FV_\theta(2\pi r_o)dx$$
$$\rightarrow W_3 = -2\pi\int_0^L \mu P_o(x)(v + z\,\phi_\theta)dx$$
$$\Rightarrow W_3 = \int_0^L (I_1 v + I_2\phi_\theta)dx \quad (41)$$
$$I_1 = -2\pi\mu P_o(x)$$
$$I_2 = -2\pi\left(\frac{h}{2}\right)\mu P_o(x)$$

The total energy is obtained as:

$$U = \int_0^L \left[U_s(x) - U_T(x)\right]dx - \int_0^L (W_1 + W_2 + W_3)dx \quad (42)$$

Euler equation for first-order functional of four variables is presented as:

$$\frac{\partial F}{\partial \Lambda_i} - \frac{\partial}{\partial x}\left(\frac{\partial F}{\partial\left(\frac{\partial \Lambda_i}{\partial x}\right)}\right) = 0 \quad (43)$$

$$\Lambda_i\,(i = 1,2,3,4,5,6) = w, \phi_x, u, \phi_z, v, \phi_\theta$$

Finally, by using the Euler equation, six differential equations of the system in matrix form are derived as:

$$[G_1]\frac{d^2}{dx^2}\{y\} + [G_2]\frac{d}{dx}\{y\} + [G_3]\{y\} = \{F\}$$
$$\{y\} = \{w \;\; \phi_x \;\; u \;\; \phi_z \;\; v \;\; \phi_\theta\}^T \quad (44)$$

The boundary conditions are written as follows:

$$x = \frac{l}{2} \rightarrow \begin{cases} \frac{du}{dx} = 0 \\ \frac{d\phi_z}{dx} = 0 \\ \frac{dw}{dx} = 0 \\ \frac{d\phi_x}{dx} = 0 \\ \frac{dv}{dx} = 0 \\ \frac{d\phi_\theta}{dx} = 0 \end{cases} \quad x = l \rightarrow \begin{cases} u = 0 \\ \phi_z = 0 \\ w = 0 \\ \phi_x = 0 \\ v = 0 \\ T = \int r\tau_{x\theta}dA_o \\ \rightarrow T = = (\mu P_o A)R \end{cases} \quad (45)$$

By applying boundary conditions, the general solution of differential equations of the system is as follows:

$$\{y\} = \sum_{i=1}^{10} c_i \{v\}_i e^{m_i x} + c_{11}x + c_{12} + \{y\}_p \quad (46)$$

3. Validation by the Finite Element Method for Thermoelastic Numerical Analysis

Abaqus finite element software has been used to validate the current analysis. The results of the thermo-elastic analysis of the functionally graded cylinder with power low distribution and uniform temperature distribution under mechanical and thermal loading, boundary conditions, and the information in Table 1 were calculated with the first order shear deformation theory and compared with those of finite element results. C3D8T element was used for finite element simulation and finally, the mentioned model converged with 50160 elements. The comparison of the results (Fig. 5) shows the appropriate accuracy of the used method.

Table1. Material property and boundary condition.

	property		*property*
150 $^\circ C$	T_i	1 m	L
70 $^\circ C$	T_o	0.04 m	R_i
200 GPa	E	0.06 m	R_o
0.3	ν	80 MPa	P_i
$1.2\times10^{-6}\frac{1}{^\circ C}$	α	30 MPa	P_o
0.01	μ	200 GPa	E
3200 rpm	w	6/5	K

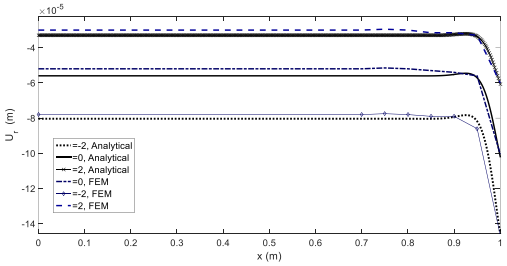

Fig. 5. Comparison of radial displacement distribution in the longitudinal direction of the cylinder obtained by FSDT and FEM methods.

4. Numerical Results

In this section, the numerical results are plotted by Matlab software based on the following data (as written in Table 2). The longitudinal results are plotted at the middle surface (z=0) and the radial results are plotted at x=0.

Table 2. Material properties, geometry, and thermal loading

geometry	Material properties		Constant	Thermal	Pressure
$L = 1m$	$\rho_{Al} = 2700\frac{Kg}{m^3}$	$k_{Al} = 237\frac{W}{mc}$	$\nu = 0.3$	$T_i = 70^o c$	$P_i = 30Mpa$
$R_i = 0.1m$	$\rho_{Sic} = 3200\frac{Kg}{m^3}$	$k_{Sic} = 120\frac{W}{mc}$	$\mu = 0.01$	$T_o = 130^o c$	$p_o = 80Mpa$
$R_o = 0.18m$	$E_{Sic} = 410Gpa$	$\alpha_{Sic} = 4\times10^{-06}\ k^{-1}$	$\omega = 3200rpm$		
	$E_{Al} = 70Gpa$	$\alpha_{Al} = 23.1\times10^{-06}\,k^{-1}$			

4.1. Friction Coefficient

Radial and axial distribution of circumferential displacements and effective stress are presented in Figures 6 and 7 for *Time=256 s* and different friction coefficients. These results show that radial and axial distribution is outward and are increased with the increase of friction coefficient. The minimum value of V_θ occurs at x=1m for all times.

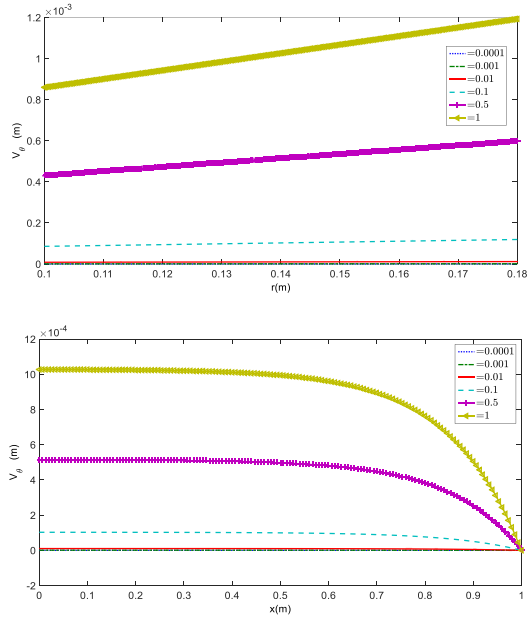

Fig. 6. The radial and axial distribution of V_θ for different friction coefficients.

As the friction coefficient increases, the effective stress also increases. As can be seen in Figure 6, the maximum value of effective stress occurs at x=1m and outer radios.

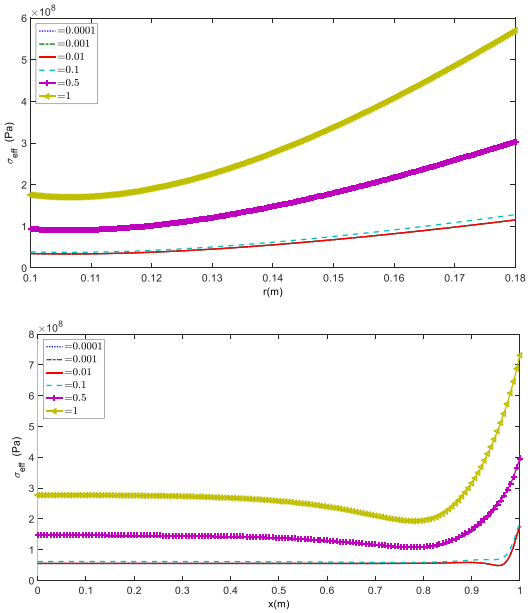

Fig. 7. The Radial and axial distributions of the effective stress for different friction coefficients.

4.2. Rotation Speed

Radial and axial distribution of displacements and effective stress are presented in Figures 8-10 for *Time=256 s* and different rotation speeds. The radial displacement is almost the same for all points. Radial displacement is zero for all rotating speeds at x=1m. As the rotating speed increases, the radial stress also increases.

As the friction coefficient increases, the environmental stress also increases

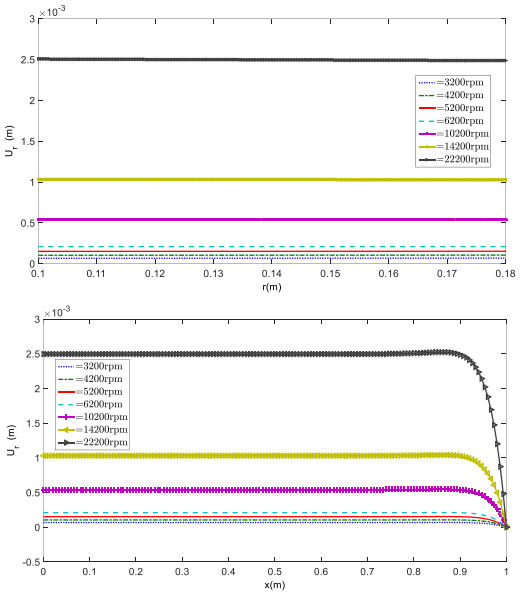

Fig. 8. Radial and axial distributions of the radial displacement for different rotation speeds.

Figures 8 and 9 show that the longitudinal displacement and effective stress increase as the rotating speed increases. On the other hand, the minimum value of W_x and effective stress occurs at about x=0.95m for all rotating speeds.

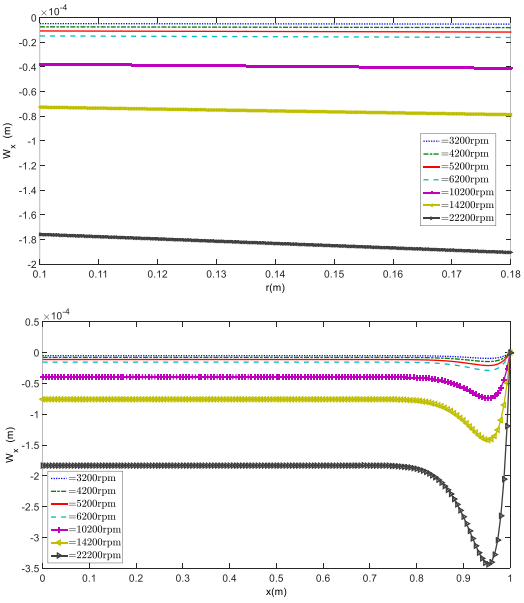

Fig. 9. Radial and axial distributions of the longitudinal displacement for different rotation speeds.

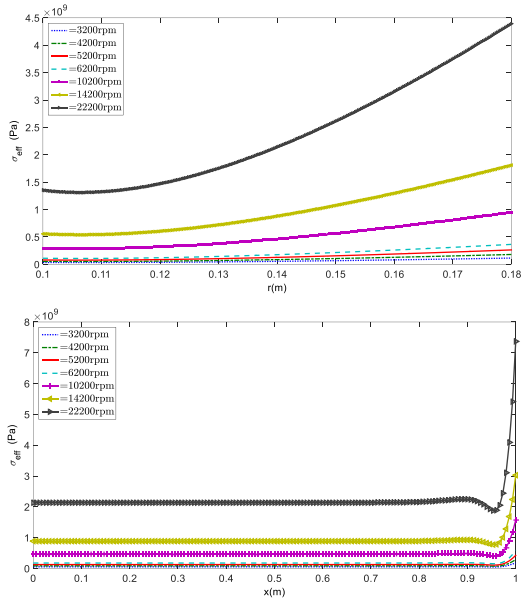

Fig. 10. Radial and axial distributions of the effective stress for different rotation speeds.

5. Conclusion

In this study, the solution of the temperature distribution was explained in detail and the resulting diagrams were shown in radial distribution. The temperature distribution approaches its steady state over time and is completely stable after about 256 seconds. As shown in the presented diagrams, the change of each of the parameters of friction coefficient and rotational speed affects displacements and effective stresses.

As the results show, increasing the amount of coefficient of friction has a direct effect on the environmental displacement and increases it, which in turn increases the effective stress. Regarding the increase of rotational speed, it can be observed that with its increase, the cylindrical barrel shape becomes more visible (in this way, positive radial displacements and longitudinal displacements increase negatively) and as a result, the amount of effective stress is combined. The minimum value of circumferential displacements and the maximum value of effective stress occur at x=1m for all times. An increase in friction coefficient has a direct effect on effective stress. Also, the increase in angular velocity has a direct effect on the radial displacement.

References

[1] Kiarasi, F., Babaei, M., Sarvi, P., Asemi, K., Hosseini, M. & Omidi Bidgoli, M., 2021. A review on functionally graded porous structures reinforced by graphene platelets. *Journal of Computational Applied Mechanics, 52* (4), pp.731-750.

[2] Babaei, M., Kiarasi, F., Asemi, K. & Hosseini, M., 2022. Functionally graded saturated porous structures: A review. *Journal of Computational Applied Mechanics, 53* (2), pp.297-308.

[3] Shishesaz, M., Shariati, M. & Hosseini, M., 2022. Size-effect analysis on vibrational response of functionally graded annular nano-plate based on nonlocal stress-driven method. *International Journal of Structural Stability and Dynamics, 22* (09), pp.2250098.

[4] Mahmoudi, R., Barati, A., Hosseini, M. & Hadi, A., 2021. Torsional vibration of functionally porous nanotube based on nonlocal couple stress theory. *International Journal of Applied Mechanics, 13* (10), pp.2150122.

[5] Kiarasi, F., Asadi, A., Babaei, M., Asemi, K. & Hosseini, M., 2022. Dynamic analysis of functionally graded carbon nanotube (fgcnt) reinforced composite beam resting on viscoelastic foundation subjected to impulsive loading. *Journal of Computational Applied Mechanics, 53* (1), pp.1-23.

[6] Shishesaz, M. & Hosseini, M., 2018. Mechanical behavior of functionally graded nano-cylinders under radial pressure based on strain gradient theory. *Journal of Mechanics, 35* (4), pp.441-454.

[7] Khoram, M.M., Hosseini, M., Hadi, A. & Shishehsaz, M., 2020. Bending analysis of bidirectional fgm timoshenko nanobeam subjected to mechanical and magnetic forces and resting on winkler–pasternak foundation. *International Journal of Applied Mechanics, 12* (08), pp.2050093.

[8] Haghshenas Gorgani, H., Mahdavi Adeli, M. & Hosseini, M., 2019. Pull-in behavior of functionally graded micro/nano-beams for mems and nems switches. *Microsystem Technologies, 25* (8), pp.3165-3173.

[9] Hosseini, M., Shishesaz, M. & Hadi, A., 2019. Thermoelastic analysis of rotating functionally graded micro/nanodisks of variable thickness. *Thin-Walled Structures, 134*, pp.508-523.

[10] Shishesaz, M., Hosseini, M., Naderan Tahan, K. & Hadi, A., 2017. Analysis of functionally graded nanodisks under thermoelastic loading based on the strain gradient theory. *Acta Mechanica, 228* (12), pp.4141-4168.

[11] Yousefi, S., Shahriari, B. & Sadeghinezhad, M.S., 2020. Elastic analysis of the rotating fgm spool drum of the axial compressor in aero gas turbine engine. *Aerospace Knowledge and Technology Journal, 8* (2), pp.55-66.

[12] Shahriari, B., Sadeghinezhad, M.S. & Yousefi, S., 2019. Thermoelastic analysis of compressor spool in turbojet engine and redesign it using functionally graded

materials with opti-mal coefficients. *Mechanics of Advanced Composite Structures, 6* (2), pp.167-179.

[13] Lezgy-Nazargah, M. & Meshkani, Z., 2018. An efficient partial mixed finite element model for static and free vibration analyses of fgm plates rested on two-parameter elastic foundations. *Struct Eng Mech, 66* (5), pp.665-676.

[14] Lezgy-Nazargah, M., 2016. A three-dimensional peano series solution for the vibration of functionally graded piezoelectric laminates in cylindrical bending. *Scientia Iranica, 23* (3), pp.788-801.

[15] Lezgy-Nazargah, M., 2015. A three-dimensional exact state-space solution for cylindrical bending of continuously non-homogenous piezoelectric laminated plates with arbitrary gradient composition. *Archives of Mechanics, 67* (1), pp.25-51.

[16] Lezgy-Nazargah, M., 2015. Fully coupled thermo-mechanical analysis of bi-directional fgm beams using nurbs isogeometric finite element approach. *Aerospace Science and Technology, 45*, pp.154-164.

[17] Arefi, M., 2014. Generalized shear deformation theory for thermo elastic analyses of the functionally graded cylindrical shells. *Structural Engineering and Mechanics, 50* (3), pp.403-417.

[18] Akbarzadeh, A. & Chen, Z., 2014. Thermo-magneto-electro-elastic responses of rotating hollow cylinders. *Mechanics of Advanced Materials and Structures, 21* (1), pp.67-80.

[19] Nasrekani, F.M. & Eipakchi, H., 2015. Nonlinear analysis of cylindrical shells with varying thickness and moderately large deformation under nonuniform compressive pressure using the first-order shear deformation theory. *Journal of Engineering Mechanics, 141* (5), pp.04014153.

[20] Ghannad, M. & Parhizkar Yaghoobi, M., 2015. A thermoelasticity solution for thick cylinders subjected to thermo-mechanical loads under various boundary conditions. *ADMT Journal, 8* (4).

[21] Jabbari, M., Nejad, M.Z. & Ghannad, M., 2015. Thermo-elastic analysis of axially functionally graded rotating thick cylindrical pressure vessels with variable thickness under mechanical loading. *International journal of engineering science, 96*, pp.1-18.

[22] Gharooni, H., Ghannad, M. & Nejad, M.Z., 2016. Thermo-elastic analysis of clamped-clamped thick fgm cylinders by using third-order shear deformation theory. *Latin American Journal of Solids and Structures, 13*, pp.750-774.

[23] Ghannad, M. & Yaghoobi, M.P., 2017. 2d thermo elastic behavior of a fg cylinder under thermomechanical loads using a first order temperature theory. *International Journal of Pressure Vessels and Piping, 149*, pp.75-92.

[24] Loghman, A., Nasr, M. & Arefi, M., 2017. Nonsymmetric thermomechanical analysis of a functionally graded cylinder subjected to mechanical, thermal, and magnetic loads. *Journal of Thermal Stresses, 40* (6), pp.765-782.

[25] Bidgoli, M.O., Arefi, M. & Loghman, A., 2021. Thermoelastic behaviour of fgm rotating cylinder resting on friction bed subjected to a thermal gradient and an external torque. *Australian Journal of Mechanical Engineering, 19* (1), pp.1-9.

[26] Omidi Bidgoli, M., Loghman, A. & Arefi, M., 2019. The effect of grading index on two-dimensional stress and strain distribution of fg rotating cylinder resting on a friction bed under thermomechanical loading. *Journal of Stress Analysis, 3* (2), pp.75-82.

[27] Omidi Bidgoli, M., Loghman, A. & Arefi, M., 2019. Three-dimensional thermo-elastic analysis of a rotating cylindrical functionally graded shell subjected to mechanical and thermal loads based on the fsdt formulation. *Journal of Applied Mechanics and Technical Physics, 60* (5), pp.899-907.

[28] Omidi Bidgoli, M., Loghman, A., Arefi, M. & Faegh, R.K., 2020. Transient stress and deformation analysis of a shear deformable fg rotating cylindrical shell made of al-sic subjected to thermo-mechanical loading. *Australian Journal of Mechanical Engineering*, pp.1-15.

[29] Praveen, G. & Reddy, J., 1998. Nonlinear transient thermoelastic analysis of functionally graded ceramic-metal plates. *International journal of solids and structures, 35* (33), pp.4457-4476.